Metallomics, 15, 2023, mfad035
https://doi.org/10.1093/mtomcs/mfad035
Advance access publication date: 18 May 2023
Paper

Mitochondria-targeted cyclometalated iridium-β-carboline complexes as potent non-small cell lung cancer therapeutic agents

Jincan Chen[1,2,3,‡], Xinhua Guo[1,2,‡], Dunhui Li[4,5], Hong Tang[1,2,3], Jie Gao[1,2], Wenzhu Yu[1,2,3], Xufeng Zhu[2,3], Zirong Sun[1], Zunnan Huang[1,*] and Lanmei Chen[1,2,*]

[1]Key Laboratory of Computer-Aided Drug Design of Dongguan City, Key Laboratory for Research and Development of Natural Drugs of Guangdong Province, School of Pharmacy, Guangdong Medical University, Dongguan, Guangdong 523808, P.R. China, [2]The Marine Biomedical Research Institute, Guangdong Medical University, Zhanjiang, Guangdong 524023, P.R. China, [3]The Marine Biomedical Research Institute of Guangdong Zhanjiang, Zhanjiang, Guangdong 524023, P.R. China, [4]Centre for Molecular Medicine and Innovative Therapeutics, Murdoch University, Perth, Western Australia 6150, Australia and [5]College of Nursing and Health, Zhengzhou University, Zhengzhou 450001, P.R. China

*Correspondence: Key Laboratory of Computer-Aided Drug Design of Dongguan City, Key Laboratory for Research and Development of Natural Drugs of Guangdong Province, School of Pharmacy, Guangdong Medical University, Dongguan, Guangdong 523808, P.R. China. (+86)0759-2388568; E-mail: zn_huang@gdmu.edu.cn (Z. Huang), lanmeichen@126.com (L. Chen).

‡These authors contributed equally to this work.

Abstract

Natural products and metals play a crucial role in cancer research and the development of antitumor drugs. We designed and synthesized three new carboline-based cyclometalated iridium complexes $[Ir(C\text{-}N)_2(PP\beta C)](PF_6)$, where PP$\beta$C = N-(1,10-phenanthrolin-5-yl)-1-phenyl-9H-pyrido[3,4-b]indole-3-carboxamide, C-N = 2-phenylpyridine (ppy, **Ir1**), 2-(2,4-difluorophenyl) pyridine (dfppy, **Ir2**), 7,8-benzoquinoline (bzq, **Ir3**), by combining iridium with β-carboline derivative. These iridium complexes exhibited high potential antitumor effects after being promptly taken up by A549 cells. Accumulating in mitochondria rapidly and preferentially, **Ir1-3** caused a series of changes in mitochondrial events, including the loss of mitochondrial membrane potential, the depletion of cellular ATP, and the elevation of reactive oxygen species, leading to significant death of A549 cells. Moreover, the activation of intracellular caspase pathway and apoptosis was further validated to contribute to iridium complexes-induced cytotoxicity. These novel iridium complexes exerted a prominent inhibitory effect on tumor growth in a three-dimensional multicellular tumor spheroid model.

Keywords: Iridium-β-carboline complexes, Mitochondria-targeted, Mitochondrial dysfunction; Apoptosis

Graphical abstract

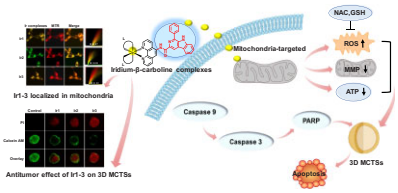

Three novel cyclometalated iridium complexes **Ir1-3** by combining iridium with β-carboline derivative were designed and synthesized, which preferentially accumulated in mitochondria, caused a series of changes in mitochondrial events, and induced A549 cell apoptosis. Meanwhile, **Ir1-3** also exerted a prominent inhibitory effect on 3D A549 multicellular tumor spheroids (MCTSs).

Introduction

Cancer is a major cause of death worldwide and is a significant barrier to patients' quality of life.[1] Under carcinogenic conditions, proto-oncogenes in local tissues are activated, and tumor suppressor genes are inactivated, thereby losing the regulation of normal cell growth and apoptosis and leading to primary tumors. Surgery, chemotherapy, and radiation therapy are the mainstream treatment options for malignant tumors, but there is still room for improvement especially in reducing side effects after chemotherapies.[2] For example, platinum-based anticancer drugs have serious drawbacks, such as renal toxicity, gastrointestinal reaction, and drug resistance. Therefore, there is an urgent and unmet need to develop novel and safer metal-based anticancer drugs with high activity. Some of the non-platinum metal complexes containing ruthenium (Ru), iridium (Ir), copper (Cu), and rhenium (Re) possess high antitumor activities, which are of great potential to be developed as substitutes for platinum drugs.[3–7] In recent years, iridium complexes have attracted extensive attention. Many studies showed that iridium complexes

Received: March 29, 2023. **Accepted:** May 17, 2023

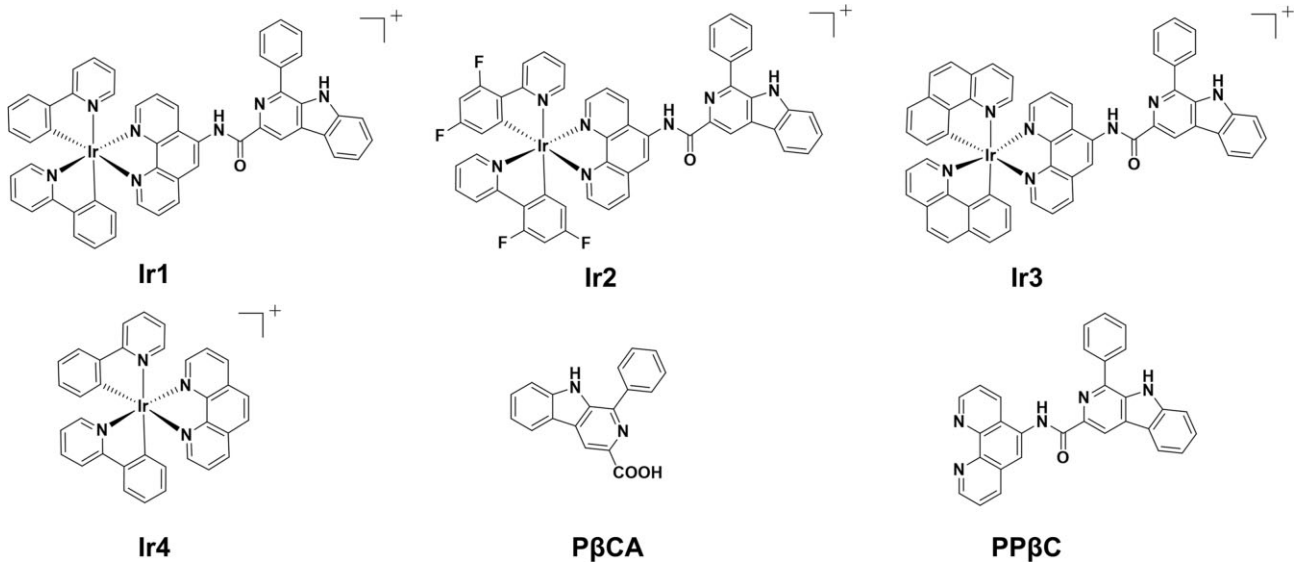

Fig. 1 Chemical structures of **Ir1-4**, PβCA, and PPβC.

exert anticancer activities through various mechanisms, including DNA binding,[8–11] protein–protein interactions,[12,13] photodynamic effects,[14–16] and targeting subcellular organelles.[3,7,17,18]

Natural products are an important source of novel drugs, drug leads, and chemical entities.[19,20] It is reported that more than 60 natural marine compounds, including leukomycin bipyridyl alkaloids, cyanobacterial bipyridyl glycosides, and polycyclic tetrameric acid macrochlorolactam have been isolated and identified from marine-derived cyanobacteria WH1-2216-6.[4] Some of these compounds exhibit cytotoxic, antibacterial, or immunosuppressive activity; however, only a few marine antitumor drugs have entered the clinic.[21,22] Alkaloids are a class of important natural compounds, with complex structures and superior biological activities, widely present in plants, animals, and marine organisms. Natural β-carboline alkaloids are mainly distributed in plants and marine organisms (sponges and soft corals). They have good biochemical activities, such as antithrombotic, antiviral, bactericidal, and anti-inflammatory effects,[23–25] making them broad application prospects in antitumor research. However, the amount of β-carboline alkaloids obtained directly from marine organisms is very small and the extraction process is complicated, which brings difficulties to their further research. Modern synthesis technology can solve this problem.

Mitochondria, commonly known as the cellular 'powerhouses', are responsible for various crucial functions in cellular processes and signaling pathways, such as energy production, generation of reactive oxygen species (ROS), biosynthetic metabolism, regulation of cell death, etc.[26–28] Tumor cells depend on glycolysis and mitochondrial metabolism to generate macromolecules, including nucleotides, lipids, amino acids, and ATP, which are essential for their survival and proliferation.[29] Due to the altered mitochondrial function in cancer cells, including mitochondrial membrane potential (MMP) and oxidative stress, mitochondria have emerged as an attractive pharmacological target for selectively killing cancer cells. In the last few years, mitochondria-targeted iridium complexes have received increasing attention as anticancer or photodynamic therapy.[24,30–32]

Our previous studies found that Ru-β-carboline derivatives complexes show antitumor effects.[33,34] To enhance the anticancer effects, we aimed to develop new Ir(III) complexes by conjugating β-carboline derivative ligands and investigating their biological functions. It is widely accepted that slight modifications in molecular geometry can significantly impact the biological activities of compounds. Following this logic, in this work, with N-(1,10-phenanthrolin-5-yl)-1-phenyl-9H-pyrido[3,4-b]indole-3-carboxamide (PPβC) as a main ligand, three new cyclometalated Ir(III) complexes $[Ir(ppy)_2(PP\beta C)](PF_6)$ (**Ir1**), $[Ir(dfppy)_2(PP\beta C)](PF_6)$ (**Ir2**), and $[Ir(bzq)_2(PP\beta C)](PF_6)$ (**Ir3**) (Fig. 1) were designed and synthesized. **Ir1-3** that combine iridium with β-carboline derivative are more effective than the other iridium complexes reported in the literature.[35] To elucidate the anticancer functions and molecular mechanisms, the cellular uptake, the accumulation site, and the antitumor effects of these three iridium complexes were investigated. **Ir1-3** induced severe mitochondria damage in A549 cells, such as MMP reduction, ATP inhibition, reactive oxygen species (ROS) production, and mitochondria morphology alteration, resulting in typical apoptosis for a large portion of tumor cells. Moreover, these novel iridium complexes exerted a prominent inhibitory effect on tumor growth in 3D multicellular tumor spheroids (MCTSs) of A549 cells.

Results and discussions

Synthesis, characterization, and stability

The synthetic route is shown in Scheme S1 in supporting information. L-tryptophan methyl ester was obtained from the amino acid L-tryptophan by methyl esterification.[36] After Pictect–Spengler cyclization, the obtained product can be carried out to the next step without purification and acylated with toluenesulfonyl chloride to obtain P-N-Ts-4H-βC, which is eliminated and aromatized under alkaline conditions to obtain compound 5 (PβC). This step is a series of elimination and aromatization reactions with mild reaction conditions and high yield. After hydrolysis, the natural product 1-phenyl-9H-pyrido[3,4-b]indole-3-carboxylic acid (PβCA) is obtained. The main ligand PPβC is obtained by condensing PβC with 1,10-phenanthroline-5-amino.[20,37] Finally, the iridium precursor $[Ir(C\text{-}N)_2Cl_2]^{-1}$(C-N = ppy, dfppy, bzq) and the main ligand PPβC are reacted to get the target cyclometalated iridium-β-carboline complexes **Ir1-3** (Fig. 1).

Table 1. Cytotoxicity assay *in vitro* (IC_{50}[a]) and $LogP_{o/w}$ values

Compounds	IC_{50}(μM)					SI[b]	$LogP_{O/W}$
	A549	Hela	HepG-2	MCF-7	BEAS-2B		
Ir1	1.0 ± 0.01	2.2 ± 0.04	3.4 ± 0. 1	5.2 ± 0.3	10.4 ± 1.4	10.4	1.9 ± 0.2
Ir2	0.7 ± 0.02	1.9 ± 0.01	2.1 ± 0.6	4.7 ± 0.9	8.8 ± 0.7	12.6	2.3 ± 0.6
Ir3	0.5 ± 0.01	1.1 ± 0.02	1.6 ± 0.4	3.7 ± 0.3	7.5 ± 0.7	15.0	3.2 ± 0.4
Ir4[c]	15.6 ± 0.6	21.5 ± 1.3	–	17.4 ± 0.3	–	–	–
PP*β*C	5.1 ± 0.1	6.3 ± 0.21	5.7 ± 0.09	5.4 ± 0.1	8.1 ± 1.3	1.6	–
P*β*CA	54.8 ± 1.7	56.9 ± 1.5	65.4 ± 2.4	79.3 ± 1.6	83.4 ± 3.1	1.5	–
Cisplatin	25.3 ± 2.4	27.4 ± 2.1	32.1 ± 2.5	21.4 ± 2.1	25.5 ± 2.5	1.0	−4.2 ± 0.9

[a]Cell viability was determined by MTT assay after treating the illustrated cells for 48 h. The data are expressed as mean ± standard deviation (Mean ± SD).
[b]SI (selectivity index) = IC_{50} (BEAS-2B)/IC_{50} (A549).
[c]The IC_{50} value of Ir4 are from ref.[34]

The UV absorption and fluorescence spectra of **Ir1-3** are shown in Figures S1–S3. In the UV absorption spectra, the peak intensity before 300 nm is caused by the intra-ligand charge transfer, and the broad peak around 350 nm is caused by the charge transfer transition from the metal center to the ligand. Under the excitation of 405 nm in the fluorescence spectra, the maximum emission wavelengths of **Ir1-3** are 586, 525, and 587 nm. At last, the complexes **Ir1-3** and the main ligand PP*β*C were characterized by elemental analysis, ESI-MS (Figs. S4–7), ^{1}H NMR (Figs. S8–S11), ^{13}C NMR (Figs. S12–14), ^{1}H-^{1}H COSY (Figs. S15–17). The ESI-MS spectrum of PP*β*C showed a characteristic peak at m/z 466.1787([M + H]$^+$) (Fig. S4). For **Ir1-3**, 966.2849, 1038.2535, and 1014.2789 [M-PF_6]$^+$ cationic peaks were detected, respectively (Figs. S5–7). These experimental values were consistent with the theoretical values, indicating the successful synthesis of above complexes. In the ^{1}H NMR spectrum of PP*β*C, proton of the amide bond at 11.16 ppm is clearly observable, indicating the successful condensation of the amide bond (Fig. S8). The purity of **Ir1-3** was higher than 97% calculated based on the chromatographic peak area ratio by reversed-phase high performance liquid chromatography (RP-HPLC) (Fig. S18).

Drug stability plays a crucial role in cellular internalization and target binding. Thus, the time-dependent absorption spectra of iridium complexes in PBS were analysed. UV-Vis absorption spectra of **Ir1-3** did not change significantly within 48 h (Fig. S19). It is important to note that upon systemic administration, iridium complexes have the ability to either precipitate or form bonds with specific biological molecules, such as various plasma proteins. This can hinder their ability to reach high-concentration biological targets. To investigate the potential binding of iridium complexes to such internal molecules, the absorption spectra of **Ir1-3** were monitored using UV-Vis spectra at 298 K, while being incubated in aqueous solutions containing bovine serum albumin (BSA). The results, as shown in Fig. S20, indicate that there was no significant change in absorbance in the UV-Vis spectra, suggesting no prominent binding of iridium complexes with plasma proteins. The inductively coupled plasma mass spectrometry (ICP-MS) results also confirmed that the **Ir1-3** did not bind to the BSA (Fig. S21).

Cytotoxicity of iridium complexes *in vitro*

The cytotoxicity of three iridium complexes against four cancer cell lines (A549, HeLa, HepG2, and MCF-7) and a normal human cell line (BEAS-2B) were determined by 3-(4,5-dimethylthiazol-2-yl)-2,5-diphenyltetrazolium bromide (MTT) assay, with clinical cisplatin as a positive control. As seen in Table 1, compared to the natural product P*β*CA and the main ligand PP*β*C, all iridium complexes showed a significantly improved broad-spectrum antitumor activity against most cancer cell lines. Among iridium complexes, **Ir3** was determined to be the most effective as demonstrated by nearly 110 times higher than that of the natural product P*β*CA and 10 times higher than that of the main ligand PP*β*C against A549 cells. Moreover, **Ir1-3** are more effective than clinical cisplatin and the iridium complex [Ir(ppy)$_2$(phen)](PF_6) (Ir4) without *β*-carboline derivative as the main ligand against all the test cancer cell lines, suggesting the main ligand PP*β*C plays a vital role *in vitro* activity of iridium complexes. Compared with cisplatin, PP*β*C, and P*β*CA, complexes **Ir1-3** exhibited much lower toxicity towards normal BEAS-2B cells. These findings suggest that **Ir1-3** possess a preferable therapeutic profile against cancer, especially lung cancer cells. The selectivity index (SI) assay, as shown in Table 1, further supported this observation, revealing a clear trend in which **Ir3** (15.0) displayed the highest selectivity index, followed by **Ir2** (12.6), **Ir1** (10.4), PP*β*C (1.6), P*β*CA (1.5), and Cisplatin (1.0). Since complexes **Ir1-3** showed better antitumor activity in lung cancer cell line A549, this cell line was chosen as the follow-up research object.

It is well known that the lipophilicity of an anticancer drug plays a crucial role in its cytotoxicity, where increased lipophilicity leads to enhanced cellular uptake and, thus, more profound cytotoxic effects.[38–40] The oil–water partition coefficients of the three iridium complexes are 1.9, 2.3, and 3.2, respectively, as listed in Table 1. The highest lipophilicity of **Ir3** may explain its prominent antitumor effects compared to the other two iridium complexes. To further evaluate the antitumor effect of **Ir3**, EdU assays were performed to assess the cell proliferation rate after the treatment of **Ir3**. As shown in Fig. S22, the intensity of red fluorescence of **Ir3**-treated A549 cells was reduced in a concentration-dependent manner, indicating a reduced DNA replication rate and a decreased proliferation of A549 cells, showing that **Ir3** can effectively inhibit the proliferation of A549 cells, which is consistent with the cytotoxicity results.

Intracellular uptake and localization of iridium complexes

Earlier research has demonstrated that the cellular localization of metal complexes and their mechanisms of action can be influenced by their lipophilicity.[41–46] Metal complexes that are more lipophilic tend to accumulate and localize in the mitochondria, while those that are more hydrophilic tend to prefer the nucleus.[44–46] The cellular uptake characteristics of transition metal-based drugs are also a crucial factor influencing their

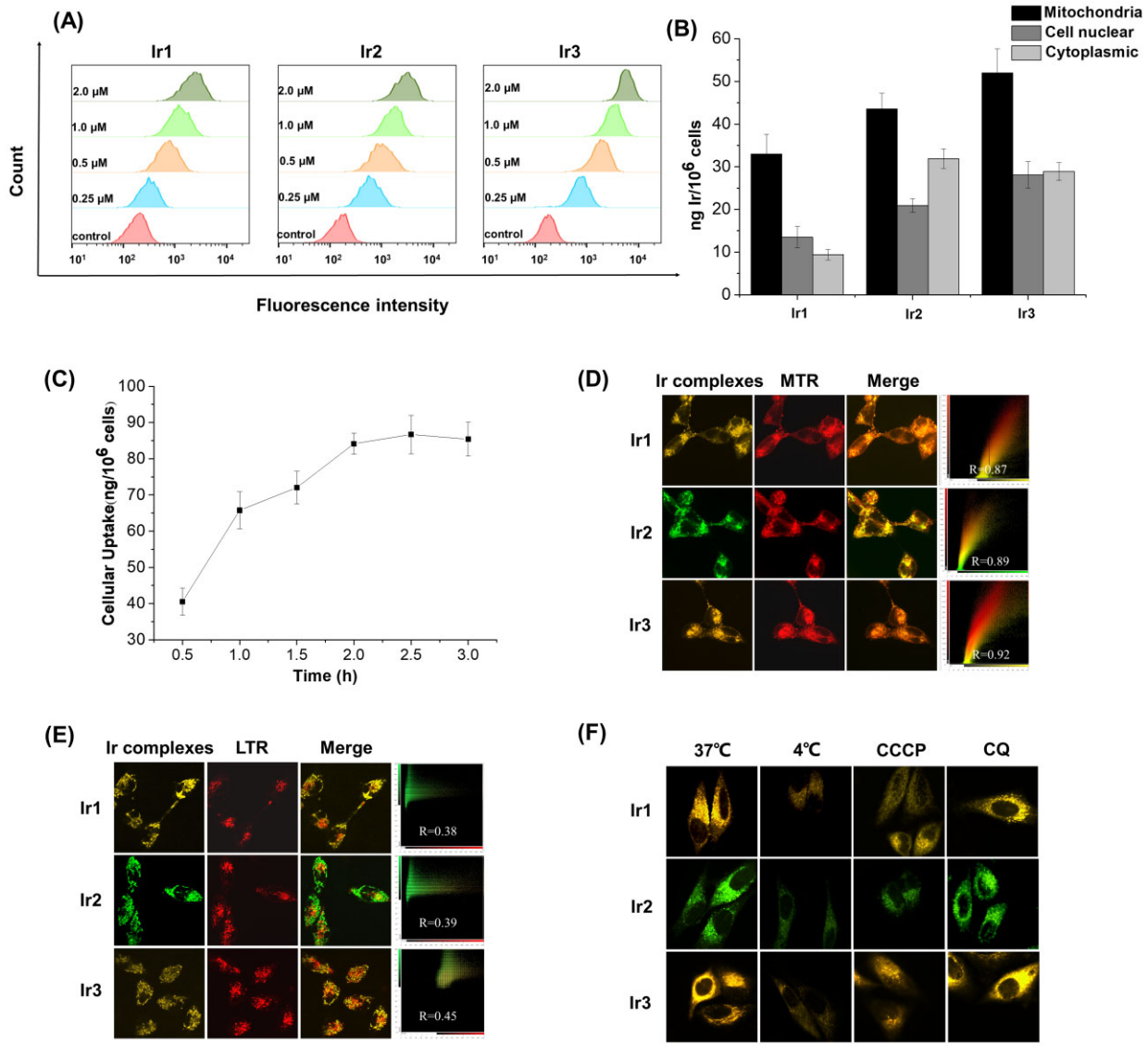

Fig. 2 (A) Flow cytometry analysis of different concentrations of **Ir1-3** uptake levels in A549 cells. (B) Subcellular distribution of Ir content in A549 cells after incubation with 0.5 μM **Ir1-3** for 24 h. (C) Cellular Ir contents were determined in A549 cells incubated with 0.5 μM **Ir3** for 3 h. (D) Confocal microscopy excited phosphorescent images of A549 cells co-labeled with **Ir1-3** (1 μM, 1.5 h) and MTR (20 nM, 20 min). (MTR) λ_{ex} = 561 nm, λ_{em} = 617 ± 36 nm, (**Ir1** and **Ir3**) λ_{ex} = 405 nm, λ_{em} = 595 ± 20 nm, (**Ir2**) λ_{ex} = 405 nm, λ_{em} = 525 ± 25 nm. (E) Confocal microscopy excited phosphorescent images of A549 cells co-labeled with **Ir1-3** (1 μM, 1.5 h) and LTR (50 nM, 0.5 h). (LTR) λ_{ex} = 561 nm, λ_{em} = 617 ± 36 nm, (**Ir1** and **Ir3**) λ_{ex} = 405 nm, λ_{em} = 595 ± 20 nm, (**Ir2**) λ_{ex} = 405 nm, λ_{em} = 525 ± 25 nm. (F) Cellular uptake mechanisms of **Ir1-3**. A549 cells were incubated with **Ir1**, **Ir2,** and **Ir3** (1 μM, 30 min), respectively, under different temperatures, pretreated with CCCP (20 μM, 1 h) or CQ (50 μM, 1 h). (**Ir1** and **Ir3**) λ_{ex} = 405 nm, λ_{em} = 595 ± 20 nm, (**Ir2**) λ_{ex} = 405 nm, λ_{em} = 525 ± 25 nm.

cytotoxicity.[35,45,47] As shown in Fig. 2A, **Ir1-3** entered cells in a concentration-dependent manner as measured by flow cytometry. ICP-MS was further used to study the cellular uptake of iridium complexes and their intracellular distribution. We detected the distribution of **Ir1-3** in cells using a mitochondrial extraction kit. As shown in Fig. 2B, the content of **Ir1-3** in mitochondria was significantly higher than in the nucleus and cytoplasm. Figure 2C showed that the intracellular **Ir3** content reached the highest value at about 2 h. Compared to other reported metal complexes, the rate of iridium complexes entering the cells is significantly fast.[48,49] The colocalization was further analysed by confocal laser scanning microscopy (CLSM). All three iridium complexes were co-stained with Mito-Tracker Red (MTR) or Lyso-Tracker Red (LTR) in A549 cells, respectively. Figure 2D and E demonstrate that the highest degree of superposition patterns occurred between the **Ir3** and MTR channels, with a Pearson's coefficient (R) of 0.92. Despite this, it was observed that the accumulation of **Ir1-3** complexes in LTR channels was poor, indicating that a significant portion of **Ir1-3** was localized within the mitochondria after being internalized by the cells (Fig. 2E). To explore the mechanisms underlying iridium complexes entering cells, A549 cells were treated with an energy inhibitor carbonyl cyanide 3-chlorophenyl hydrazone (CCCP), and an endocytosis inhibitor chloroquine (CQ), respectively. As shown in Fig. 2F, the fluorescence intensity was significantly reduced in A549 cells after being treated with CCCP compared to the control group (37°C), indicating the existence of an energy-dependent mechanism. However, no significant changes in cellular uptake in cells pretreated with CQ. These results suggest that iridium complexes enter cancer cells through an energy-dependent non-endocytosis

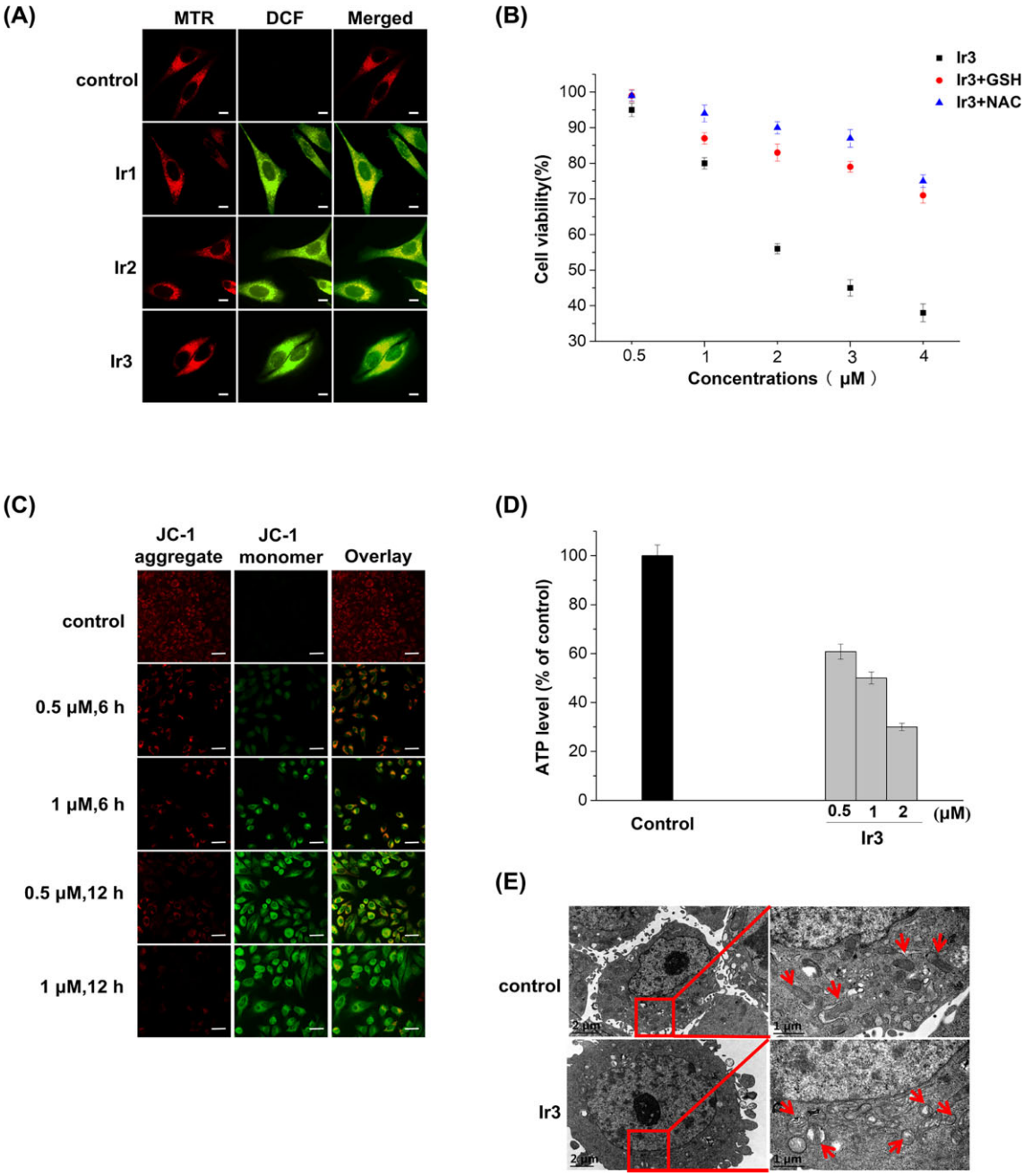

Fig. 3 (A) Generation of mitochondrial ROS caused by **Ir1-3** treatment. A549 cells were treated with **Ir1-3** at 0.5 μM for 3 h, respectively. Then, the cells were co-stained with H_2DCFDA and MTR for CLSM observation. (DCF: λ_{ex} = 488 nm; λ_{em} = 525 ± 25 nm; MTR: λ_{ex} = 561 nm; λ_{em} = 617 ± 36 nm). (B) Cell viability assay after A549 cells treatment with 1 μM **Ir3** for 24 h in the absence or presence of GSH or NAC. GSH: 5 mM; NAC: 10 mM. (C) CLSM analysis of cellular MMP level by JC-1 staining after treatment with **Ir3** at 0.5, 1 μM for 6 or 12 h, respectively. (JC-1 aggregate, λ_{ex} = 585 nm, λ_{em} = 595 ± 20 nm; JC-1 monomer, λ_{ex} = 488 nm, λ_{em} = 525 ± 25 nm). (D) Intracellular ATP levels after treatment with **Ir3** at the indicated concentrations. (E) Representative TEM images showing the morphological features in A549 cells after treatment with 0.5 μM **Ir3** for 24 h. Red arrows: impaired mitochondria.

pathway, consistent with previously reported other iridium complexes.[7,50,51]

Production of reactive oxygen species and mitochondrial dysfunction

Mitochondria, which are the powerhouse of cells, participate in several crucial cellular processes, including cell differentiation, information transmission, and apoptosis, and are the primary source of ROS, which is closely related to mitochondrial damage.[52–56] Using the ROS probe H_2DCF-DA, the production of ROS in mitochondria was detected by CLSM. As demonstrated in Fig. 3A, the fluorescence of DCF overlapped well with that of MTR, indicating that mitochondria are the major ROS-generating sites. Figure S23 showed the changes of ROS measured by the microplate reader, indicating that the intracellular ROS after iridium complexes treatment increases in a time- and concentration-dependent manner. Three iridium complexes **Ir1-3** caused an elevated production of ROS, and it was further found that this ROS is mainly produced from mitochondria (Fig. 3A). To demonstrate the effect of ROS on cell viability, two antioxidants N-acetyl-L-cysteine

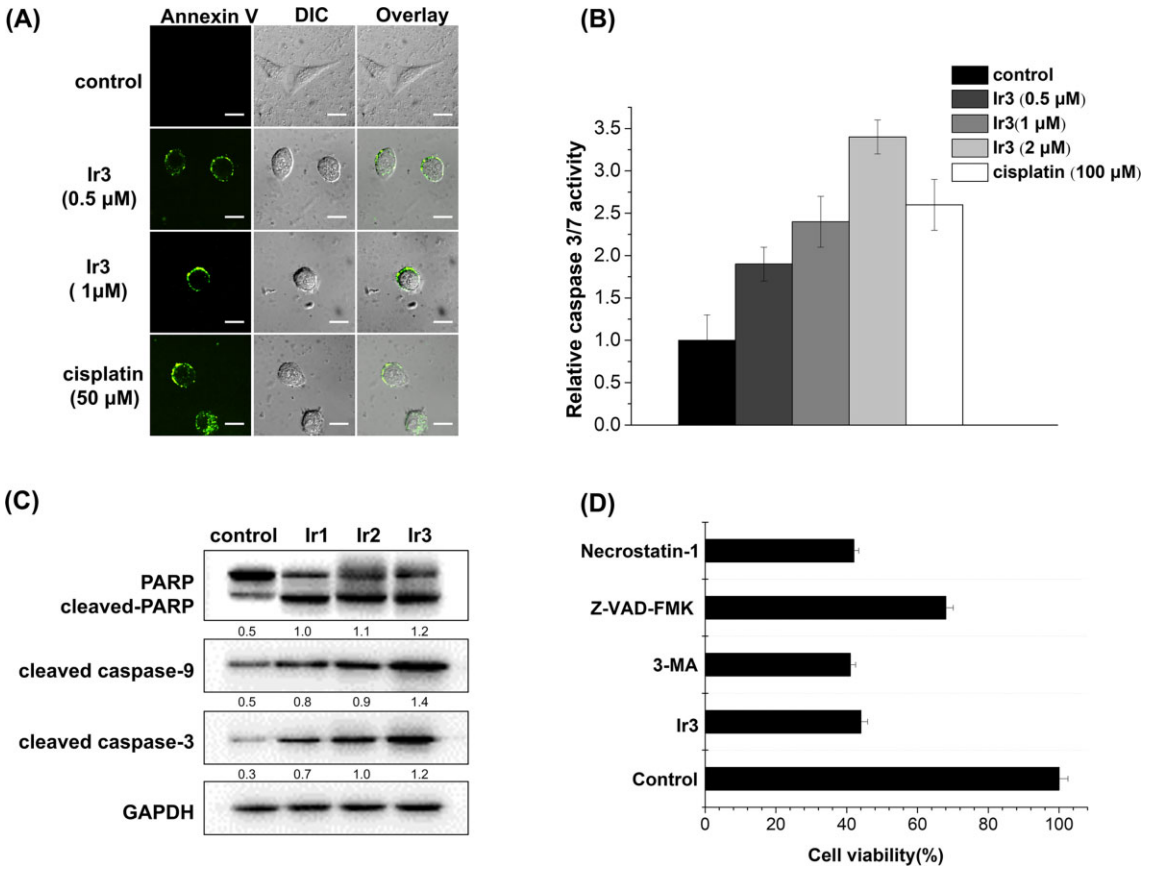

Fig. 4 (A) Representative confocal images of annexin V labeled A549 cells after treatment with 0.5 or 1 μM complex **Ir3** or 50 μM cisplatin for 24 h. (Annexin V: $\lambda_{ex} = 488$ nm; $\lambda_{em} = 525 \pm 25$ nm). (B) Caspase activities were measured by using specific fluorescent substrates for caspase-3/7. (C) The expression levels of PARP and cleaved caspase-3/9 and cleaved PARP were evaluated with 0.5 μM **Ir1-3** treatment for 24 h, and GAPDH was used as an internal control. (D) Cell viability detection after treatment with 0.5 μM **Ir3** for 24 h in the absence or presence of various inhibitors. 3-MA: 1 mM; Z-VAD-FMK: 25 μM; Necrostatin-1: 60 μm.

(NAC) and glutathione (GSH) were used. As evidenced in Fig. 3B, **Ir3** induced significant cell death in a concentration-dependent manner and the cell death was rescued by antioxidants.

We have previously found that iridium complexes **Ir1-3** can accumulate in mitochondria, and the changes in MMP can be detected after staining live cells with 5,5′,6,6′-tetrachloro-1,1′,3,3-tetraethylbenzimidalylcarbo cyanine iodide (JC-1) as a fluorescent probe.[57,58] Compared to the control, the **Ir3** treatment caused a red-to-green color shift in most of the treated cells, indicating the loss of MMP (Fig. 3C).

Considering the role of mitochondria in cellular energy production and the effects of loss of membrane potential on mitochondrial ATP production, ATP assays were performed. We found that intracellular ATP levels were significantly decreased concentration-dependent (Fig. 3D). The ultrastructural changes of **Ir3**-treated A549 cells were further analyzed using transmission electron microscopy (TEM). Figure 3E illustrated that the chromatin of A549 cells treated with **Ir3** did not change significantly; however, the mitochondrial structure was swollen, the cristae folds weakened, and the overall rounded and shortened, indicating that mitochondrial damage caused structural and morphological changes. These findings suggested that **Ir3** preferentially accumulates in the mitochondria and can rapidly and effectively affect the mitochondria's functions in ROS and cellular ATP production and alter the mitochondrial morphology.

Underlying mechanisms of Ir3-induced cell death

The potent anticancer activity of iridium complexes has prompted us to explore the underlying mechanisms. To investigate whether **Ir3** induces apoptosis of A549 cells, AO/EB double staining was applied (Fig. S24). AO is a critical dye that exhibits green fluorescence and has the ability to stain both live and dead cells; EB, as a nuclear dye, cannot penetrate normal cells. Only when the permeability of the cell membrane is changed can EB enter the cells and emit red fluorescence.[59] Control cells exhibited normal morphology with a uniform green fluorescence, while preincubation of cells with **Ir3** complex resulted in the observation of orange or red fluorescence, which were distinct morphological features of apoptosis. The AO/EB double staining results suggested that the **Ir3** complex could induce apoptosis of A549 cells.

In addition, to further study if there are **Ir3**-induced early apoptosis events, Annexin V staining was conducted, which can bind to phosphatidylserine (PS) exposed to extracellular space. As shown in Fig. 4A, PS of both **Ir3** and cisplatin-treated cells were stained, indicating that both complex **Ir3** and cisplatin induced A549 cells apoptosis. Furthermore, since caspase plays a crucial role in the initiation and performance of apoptosis, and caspase activation is considered one of the essential features of apoptosis,[60,61] to further confirm cell apoptosis induced by **Ir3**, the activity of caspase-3/7 was examined using specific fluorescent substrates. Figure 4B

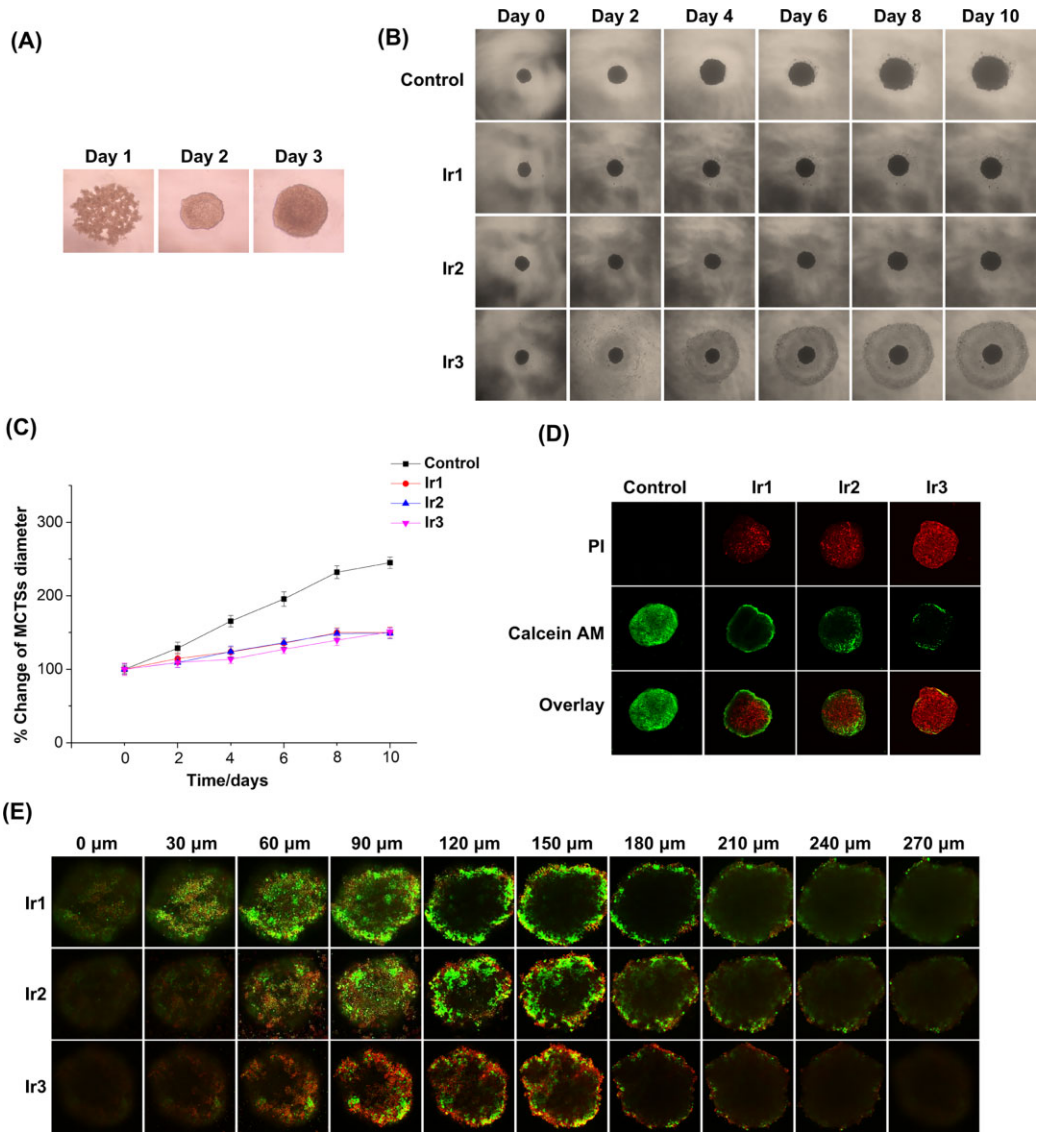

Fig. 5 (A) Formation of A549 tumor spheroids within 3 days. (B) MCTSs were treated with 0.5 μM **Ir1-3** for 10 days, respectively. (C) After treatment with 0.5 μM **Ir1-3**, A549 MCTSs were routinely monitored for regrowth inhibition. (D) Calcein AM and PI dual-staining of MCTSs after treated with 0.5 μM **Ir1-3** for 48 h. (E) Z-stack images (top) and 3D z-stacks (bottom) of Calcein-AM (λ_{ex} = 488 nm, λ_{em} = 525 ± 25 nm)/PI (λ_{ex} = 535 nm, λ_{em} = 617 ± 36 nm) double staining observed by CLSM after incubation of A549 MCTSs with 0.25 μM **Ir1-3** over 48 h, respectively. Z-axis image scan from the top to the bottom of an intact spheroid every 30 mm.

indicates that the pre-incubation of A549 cells with **Ir3** complex resulted in a significant and concentration-dependent increase in caspase-3/7 activities. Notably, 1 μM **Ir3** activated caspase-3/7 levels comparable to 100 μM cisplatin.

To further study the signaling pathway of apoptosis induced by the synthesized iridium complexes, the effects of the three iridium complexes on the protein expression levels of PARP, and cleaved PARP, cleaved caspase-3/9, were studied by western blotting assays. As shown in Fig. 4C, compared to the control group, 0.5 μM **Ir1-3** complexes increased the protein expression levels of cleaved-PARP and cleaved caspase-3/9 in A549 cells after 24 h treatment. The results further verified that the three iridium complexes could induce the apoptosis pathway in A549 cells.

To exclude that non-programmed cell death is involved in **Ir3**-induced cell death, a necrosis inhibitor (Necrostatin-1), an autophagy inhibitor (3-MA), and an apoptosis inhibitor (Z-VAD-FMK) were used. As shown in Fig. 4D, neither Necrostatin-1 nor 3-MA could prevent **Ir3**-induced apoptosis; however, adding Z-VAD-FMK increased the cell survival rate. Thus, the above results confirmed that iridium complexes induce cell death through the apoptosis pathway.

Iridium complexes-induced antitumor effects on 3D multicellular tumor spheroids (MCTSs)

Multicellular tumor spheroids (MCTSs) possess the ability to develop a necrotic core, a quiescent intermediate region, and a proliferating periphery region, which allows them to closely resemble the microenvironment of a tumor when compared to a monolayer cell system[62,63]. As a result, the use of three-dimensional MCTS models for drug screening has gained significant attention.[64] To further investigate the biological effect of **Ir1-3** on 3D MCTSs, A549 MCTSs with a diameter of approximately 200 μm were successfully constructed (Fig. 5A). Then, the growth rate of MCTSs after the treatment of **Ir1-3** at 0.5 μM was monitored. The cell

spheroid treated with **Ir1-3** were significantly smaller than the control group within 10 days (Fig. 5B). Unlike other groups, obvious cell debris appeared around the spheroids after **Ir3** treatment. Besides, as shown in Fig. 5C, the diameter of the cell spheroid changed slowly, displaying that the growth of the cell spheroid was significantly inhibited. To further assess the cytotoxicity of complexes **Ir1-3**–A549 MCTSs, A549 MCTSs were stained with Calcein-AM/propidium iodide (PI) after treatment with 0.5 μM **Ir1-3**, respectively. As shown in Fig. 5D, untreated MCTSs, composed mainly of viable cells, were observed to emit extensive green fluorescence in A549 cells. Conversely, incubation with 0.5 μM **Ir1-3** resulted in significant enhancement of PI red and weak green fluorescence in MCTSs, indicating severe cellular damage in a majority of cancer cells. When the concentration of complexes was reduced to 0.25 μM, the red fluorescence of **Ir3**-treated A549 MCTSs was still strong (Fig. 5E), suggesting that complex **Ir3** exhibited good antitumor activity even at low concentration.

Conclusions

In summary, we designed and synthesized three novel Ir(III) complexes **Ir1-3** with marine-derived β-carboline as the parent after structural modification and optimization. Complexes **Ir1-3** showed significant anticancer activities, among which **Ir3** was the most prominent. Synthesized Ir(III) complexes **Ir1-3** can enter A549 cells through an energy-dependent non-endocytosis pathway, and preferentially accumulate in the mitochondria and impair mitochondrial functions as evidenced by the loss of MMP, the reduction of cellular ATP production, and the increase of ROS in mitochondria. These iridium complexes can induce remarkable cell death through the caspase-mediated apoptosis pathway *in vitro*. Using the 3D MCTSs model to simulate the conditions of solid tumor proliferation *in vivo*, the results showed that **Ir1-3** had a notable effect against the growth tumor spheres. Our findings indicated that the synthesized novel three iridium complexes targeted mitochondria, significantly inhibited tumor growth, and had substantial application prospects in targeted therapy of tumors.

Experimental section

Synthesis and characterization

Synthesis of complexes

(1) Synthesis of compound 2 (Trp-OCH_3)

Compound 2 was prepared following a published protocol.[65]

(2) Synthesis of compound 3 (P-4H-βC)

Compound 3 was synthesized according to references[65,66]; i.e. compound 2 (1.019 g, 4 mmol) was added to the reaction tube, followed by benzaldehyde (408 μL, 4 mmol) and dissolved in 15 mL of isopropanol. Under argon protection, the mixture was heated to reflux at 90°C for 10 h, the obtained liquid was distilled under reduced pressure to remove the solvent, stirred with benzene, suction filtered, and dried to obtain a pale-yellow solid with a yield of 92.3%.

(3) Synthesis of compound 4 (P -N-Ts-4H-βC)

Compound 3 (1.23 g, 4 mmol) was dissolved in dichloromethane, 350 μL of pyridine and p-toluenesulfonyl chloride (0.76 g, 4 mmol) was added at −8°C, then stirred at room temperature for 4 h, and the solvent was distilled off under reduced pressure. It was washed with 10 mL of 10% potassium carbonate solution, dried over anhydrous magnesium sulphate, washed with petroleum ether, and filtered with suction to obtain compound 4, a yellow solid yielding 86.8%.

(4) Synthesis of compound 5 (PβC)

Substance 4 (1.84 g, 4 mmol) was dissolved in dimethyl sulfoxide, potassium carbonate (0.69 g, 5 mmol) was added, and the mixture was heated to reflux at 100°C for 5 h. After the reaction was completed, the liquid was cooled to room temperature, 100 mL of water was added, stirred and suction filtered, washed with water, and dried to obtain the product, compound 5, with a yield of 89.1%.

(5) Synthesis of compound 6 (PβCA)

Compound 5 (1.21 g, 4 mmol) was dissolved in a mixed solution of ethanol and water (30 mL, 2:1, v/v), sodium hydroxide (0.40 g, 12 mmol) was added, and refluxed at 100°C. The pH of the reacted solution was adjusted to 5 with 5 M HCl, suction filtered, and dried to obtain a yellow solid with a yield of 85.5%.

(6) Synthesis of compound 7 (PPβC)

Compound 7 was prepared following a published procedure.[67] Compound 6 (1.15 g, 4 mmol) was added to 1-Hydroxybenzotriazole (0.81 g, 6 mmol), N-Ethyl-N-(1-methylethyl)-2-propanamine (400 uL), and 1,10-phenanthroline-5-amino (0.78 g, 4 mmol). After 2 h of reaction at room temperature, 1-Ethyl-3-(3-dimethylaminopropyl) carbodiimide hydrochloride (1.15 g, 6 mmol) was added, and the reaction was continued at room temperature for 21 h. The solvent was removed, washed with water, and the resulting yellow precipitate was filtered. The crude product was applied to a silica gel column for a white solid.

PPβC: ^{1}H NMR (400 MHz, DMSO-d_6) δ 12.04 (s, 1H), 11.16 (s, 1H), 9.17 (dd, J = 4.3, 1.6 Hz, 1H), 9.08 (dd, J = 4.3, 1.7 Hz, 1H), 9.04 (s, 1H), 8.55 (ddd, J = 10.3, 8.2, 1.7 Hz, 2H), 8.50 (d, J = 7.9 Hz, 1H), 8.46 (s, 1H), 8.39—8.31 (m, 2H), 7.87 (dd, J = 8.4, 4.2 Hz, 1H), 7.79 (dd, J = 8.1, 4.3 Hz, 1H), 7.73 (q, J = 8.1, 7.7 Hz, 3H), 7.64 (q, J = 7.5 Hz, 2H), 7.37 (t, J = 7.5 Hz, 1H).

(7) Synthesis of compound $Ir_2(L)_4Cl_2$

We followed the procedure of an established synthesis[68,69] and obtained a pure yellow crystal of the dichloro-bridged $Ir_2(L)_4Cl_2$ dimer (L = 2-phenylpyridine, 2-(2,4-difluorophenyl) pyridine, 7,8-benzoquinoline).

(8) Synthesis of compound **Ir1-3**

$Ir_2(L)_4Cl_2$ (2 mmol) and PPβC (1.86 g, 4 mmol) were dissolved in a mixed solution of dichloromethane: methanol (2:1, v/v) and refluxed for 4 h under argon protection. After the reaction, the solution was cooled to room temperature, CH_2Cl_2 was removed, and 20 mL of KPF6-saturated aqueous solution was added. After standing, filter, vacuum dry, and purify to obtain **Ir1-3**. The yellow precipitate was filtered, washed with water and dried in a vacuum.

Ir1: ^{1}H NMR (400 MHz, DMSO-d_6) δ 12.11 (s, 1H), 11.36 (s, 1H), 9.08 (s, 1H), 8.94 (dd, J = 8.4, 1.4 Hz, 1H), 8.92—8.88 (m, 1H), 8.87 (s, 1H), 8.52 (d, J = 7.9 Hz, 1H), 8.34—8.25 (m, 5H), 8.17—8.15 (m, 1H), 8.15—8.11 (m, 1H), 8.04 (dd, J = 8.3, 5.0 Hz, 1H), 7.98 (d, J = 7.8 Hz, 2H), 7.93—7.85 (m, 4H), 7.75 (d, J = 8.2 Hz, 1H), 7.67 (d, J = 7.3 Hz, 1H), 7.52 (t, J = 4.6 Hz, 2H), 7.37 (s, 2H), 7.11—7.06 (m, 2H), 7.03 (t, J = 6.7 Hz, 2H), 7.00—6.94 (m, 2H), 6.33 (d, J = 7.4 Hz, 2H). ESI-MS(CH_3CN): m/z calc. for ([M-PF_6]$^+$) 966.25; found: 966.28. ^{13}C NMR (101 MHz, DMSO-d_6) δ 167.37, 164.84, 151.31, 150.54, 150.27, 150.19, 149.57, 149.53, 147.04, 144.53, 144.49, 142.24, 141.49, 139.23, 138.95, 138.82, 137.75, 135.26, 134.94, 134.58, 131.79, 131.33, 130.74, 130.68, 129.75, 129.39, 128.14, 127.79, 127.21, 125.58, 124.47, 124.40,

124.32, 122.90, 122.68, 121.66, 121.01, 120.52, 120.47, 114.54, 113.36. UV-Vis (λ/nm, $\varepsilon/M^{-1}\bullet cm^{-1}$) (PBS): 280 (69 000), 348 (32 150). Elemental analysis calcd (%) for $C_{52}H_{35}F_6IrN_7OP$: C, 56.15; H, 3.15; N, 8.82; found: C, 54.18; H, 3.16; N, 8.84.

Ir2: ^{1}H NMR (400 MHz, DMSO-d_6) δ 12.09 (s, 1H), 11.40 (s, 1H), 9.08 (s, 1H), 8.97 (dd, J = 13.1, 8.3 Hz, 2H), 8.90 (s, 1H), 8.51 (d, J = 7.9 Hz, 1H), 8.38 (s, 1H), 8.34 (d, J = 7.4 Hz, 4H), 8.29—8.24 (m, 1H), 8.14 (dd, J = 8.5, 5.1 Hz, 1H), 8.00 (d, J = 7.1 Hz, 3H), 7.75 (s, 1H), 7.73—7.62 (m, 4H), 7.59 (d, J = 6.1 Hz, 2H), 7.38 (t, J = 7.4 Hz, 1H), 7.16—7.08 (m, 2H), 7.04 (s, 2H), 5.75 (dd, J = 8.3, 2.4 Hz, 2H). ESI-MS (CH_3CN): m/z calc. for ($[M\text{-}PF_6]^+$) 1038.22; found: 1038.25. ^{13}C NMR (101 MHz, DMSO-d_6) δ 164.84, 164.65, 164.54, 164.52, 163.38, 163.31, 162.60, 162.47, 162.13, 162.11, 162.00, 160.02, 159.89, 154.65, 154.59, 154.37, 154.31, 151.97, 150.77, 150.28, 146.72, 144.16, 142.25, 141.52, 140.45, 139.35, 138.92, 137.75, 135.50, 135.28, 134.67, 131.47, 130.68, 129.75, 129.41, 128.33, 128.23, 128.08, 127.52, 124.99, 124.90, 123.94, 123.92, 123.77, 123.74, 122.65, 121.66, 121.00, 120.53, 114.55, 114.09, 113.93, 113.37, 99.92, 99.64, 99.38. UV-Vis (λ/nm, $\varepsilon/M^{-1}\bullet cm^{-1}$) (PBS): 281 (57 950), 348(27 950). Elemental analysis calcd (%) for $C_{52}H_{31}F_{10}IrN_7OP$: C, 52.74; H, 2.62; N, 8.28; found: C, 52.71; H, 2.61; N, 8.30.

Ir3: ^{1}H NMR (400 MHz, DMSO-d_6) δ 12.08 (s, 1H), 11.39 (s, 1H), 9.07 (s, 1H), 8.90 (s, 3H), 8.57—8.50 (m, 3H), 8.34—8.31 (m, 2H), 8.26 (dd, J = 5.0, 1.2 Hz, 1H), 8.13 (dd, J = 5.1, 1.3 Hz, 1H), 8.04—7.99 (m, 5H), 7.96—7.93 (m, 1H), 7.91 (d, J = 3.2 Hz, 1H), 7.89 (d, J = 3.3 Hz, 1H), 7.75 (s, 1H), 7.68 (d, J = 7.6 Hz, 3H), 7.60 (d, J = 7.7 Hz, 3H), 7.48 (ddd, J = 8.1, 5.4, 1.3 Hz, 2H), 7.40—7.36 (m, 1H), 7.25 (s, 2H), 6.35 (dd, J = 7.2, 3.6 Hz, 2H). ESI-MS(CH_3CN): m/z calc. for ($[M\text{-}PF_6]^+$) 1014.25; found: 1014.28. ^{13}C NMR (101 MHz, DMSO) δ 164.79, 156.89, 151.82, 150.66, 149.31, 147.47, 147.34, 147.05, 144.92, 142.24, 141.48, 140.89, 140.84, 138.93, 138.80, 138.09, 137.74, 135.27, 134.83, 134.55, 134.25, 131.34, 130.67, 130.21, 130.00, 129.74, 129.40, 129.36, 129.13, 128.06, 127.75, 127.23, 127.20, 124.71, 123.29, 123.22, 122.65, 121.65, 120.99, 120.91, 120.28, 114.53, 113.35. UV-Vis (λ/nm, $\varepsilon/M^{-1}\bullet cm^{-1}$) (PBS): 260 (76 000), 340(34 050). Elemental analysis calcd (%) for $C_{56}H_{35}F_6IrN_7OP$: C, 57.97; H, 3.02; N, 8.45; found: C, 57.99; H, 3.01; N, 8.43.

UV-vis and fluorescence spectroscopy analysis

The UV-Vis absorption spectra of **Ir1-3** at 293 K were obtained using PBS as the solvent, and recorded on a Perkin Elmer Lambda 850 spectrophotometer. The samples were excited at 405 nm, and the emission wavelengths were recorded on a Perkin Elmer LS-55 spectrofluorometer, ranging from 450 to 750 nm.

Stability assay

The stability of the **Ir1-3** complexes was measured by UV-Vis spectroscopy and ICP-MS according to our previous reports.[48,70]

Cell lines and culture conditions

The Experimental Animal Center of Sun Yat-Sen University (Guangzhou, China) provided four cancer cell lines, A549, HepG2, MCF-7, and HeLa, as well as a normal cell line, BEAS-2B. All the cell lines were cultured in DMEM media supplemented with 10% FBS and incubated in a 5% CO_2 incubator at 37 °C.

In vitro cytotoxicity assay

To assess the cytotoxicity of **Ir1-3** and other control compounds, the MTT assay was utilized. The cells were seeded overnight in 96-well plates at a density of 4 × 10^3 cells per well. Next, the tested compounds, **Ir1-3**, and the same amount of DMSO as the negative control were added to the wells. The plates were incubated for 48 h before the addition of MTT dye stock solution (10 μL, 1 mM) to each well. After a 4 h incubation period, DMSO (150 μL/well) was used to solubilize the fresh formazan. The optical density of each well was then measured at a wavelength of 570 nm using a microplate spectrophotometer. The analysis of absorbance data provided the IC_{50} values.

EdU staining to detect cell proliferation

EdU is a thymidine analog, a new nucleoside marker that can replace thymidine (T) during DNA replication. After a cell cycle of EdU culture, EdU will enter all cells and act as proliferating cells-sensitive fluorescent markers. A549 cells were evenly seeded in a confocal dish, and the complex was added after the cells were attached to the dish for 12 h. These cells were stained with EDU, followed by infiltration with 0.5% Triton X-100 for 20 min and washing with 3% BSA. Hoechst 33 342 was stained in the dark for 10 min, washed with PBS, and observed and photographed under an inverted fluorescence microscope.

Lipophilicity measurements

$LogP_{o/w}$ values were determined using a protocol that was previously described.[70] Equal amounts of H_2O and octanol were mutually saturated for 12 h. **Ir1-3** were added to a mixture of octanol/H_2O aqueous solution (1:1, v/v), respectively, and then shaken at 37 °C, 200 rpm for 24 h. The oil and water phases were separated by centrifugation (3000 rpm, 10 min) and collected. To prepare the samples, 100 μL of the aqueous phase and 100 μL of the oil phase were taken and treated with 10% HNO_3 and 20% H_2O_2, respectively, overnight. The resulting solutions were then brought up to a final volume of 5 mL each. The ICP-MS (NEXION-300X, PerkinElmer, USA) was utilized to measure the Ir(III) content in the aqueous and oil phases. $LogP_{o/w}$ values were calculated using the equation $LogP_{o/w} = Log\ ([Ir]_o/[Ir]_w)$.

Cellular uptake

A549 cells were seeded in 60 mm tissue culture dishes and incubated for 24 h before treatment with **Ir3**. Following treatment, the cells were trypsinized, collected in centrifugal tubes, and washed thrice with cold PBS. The cell pellets were digested in a mixture of HNO_3 and H_2O_2 for 24 h and diluted to 4 mL with ultrapure water. The amount of iridium taken up by the A549 cells was determined by ICP-MS using a 100 ng/mL iridium standard solution.

Subcellular distribution of ir(III) complexes

A549 cells were seeded in 60 mm tissue culture dishes and incubated for 12 h before treatment with **Ir1-3** for 24 h, respectively. Cellular fractions, including nuclear, mitochondrial, and cytoplasmic fractions, were extracted using the Cell Mitochondria Isolation Kit (Beyotime).[71,72] The harvested cells were resuspended in mitochondrial isolation buffer, homogenized, and centrifuged at 600 g for 10 min to obtain the pellet (nucleus fraction). The remaining supernatant was centrifuged at 11 000 g for 10 min at 4 °C to obtain the supernatant (cytoplasmic fraction) and pellet (mitochondrial fraction). The fractions were then digested using HNO_3 and H_2O_2 for 24 h, diluted to 4 mL with ultrapure water. The iridium content in each fraction was determined by ICP-MS, using a 100 ng/mL iridium standard solution.

Colocalization assay

A549 cells were initially seeded into 35 mm confocal dishes and incubated at 37 °C for 12 h. Afterward, **Ir1-3** (1 μM) was added, respectively, and the cells were incubated for an additional 3 h. Subsequently, the cells were washed with PBS twice and incubated with fluorescent probes, Mito-Tracker Red (MTR), and

Lyso-Tracker Red (LTR), at 37 °C for 30 min each. The cells were then rewashed with PBS and observed using CLSM with a 60× oil-immersion objective lens. The excitation/emission wavelengths for **Ir1** and **Ir3** were set at 405 nm/595 ± 20 nm, while for **Ir2**, they were set at 405 nm/525 ± 25 nm. The excitation/emission wavelengths for MTR and LTR were set at 561 nm/617 ± 36 nm.

Cellular uptake mechanism study

To investigate the cellular uptake mechanism of **Ir1-3**, CLSM imaging was used. After being pretreated with various inhibitors under different conditions, A549 cells were incubated with **Ir1-3**. Then, the cells were washed with PBS three times and observed using CLSM. For the temperature influence study, HeLa cells were treated with **Ir1-3** (0.5 μM) in the dark for 2 h at 37 °C and 4 °C, respectively. In the metabolic inhibition study, A549 cells were pretreated with carbonyl cyanide 3-chlorophenylhydrazone (CCCP, 20 mM) or chloroquine (CQ, 50 μM) for 1 h and then exposed to **Ir1-3** (0.5 μM) in the dark for 2 h at 37 °C.

Cellular ROS detection

A549 cells were treated with the iridium complexes at the indicated concentrations for 3 h. The cells were harvested and incubated with 10 μM H_2DCFDA and MTR for 15 min at 37°C in the dark and then photographed using an inverted fluorescence microscope.

MMP measurement

MMP was analyzed using CLSM. A549 cells were incubated with different concentrations (0.5, 1.0 μM) of **Ir3** at different time points (6, 12 h). Cells were incubated in a complete medium containing 10 mg/mL JC-1 for 30 min and washed twice with PBS; images of the cells were photographed immediately by CLSM.

Intracellular ATP detection

The experimental procedure was conducted by a previously published method.[73] The Cell Titer-Glo® Luminescent Cell Viability Assay kit (G7570, Promega, USA) was used to measure the cellular ATP level according to the manufacturer's instructions.

Transmission electron microscopy (TEM) detection

A549 cells were grown in 60 mm tissue culture dishes for 12 h, followed by treatment with **Ir3** (0.5 μM). After 24 h of incubation, the cells were collected and fixed overnight in PBS containing 2.5% glutaraldehyde (pH = 7.4) at 4°C. The cells were then treated with osmium tetroxide, stained with uranyl acetate and lead citrate solution, and finally observed under a transmission electron microscope (JEM-1400, JEOL, Japan).

AO/EB staining assay

A549 cells were cultured in 35 mm confocal dishes and treated with or without iridium complexes for 24 h. After incubation, the cells were washed twice with cold PBS, stained with AO/EB solutions at a concentration of 100 μg/mL, and observed using an inverted fluorescence microscope.

Annexin V staining assay

The experiment was carried out following the manufacturer's instructions. A549 cells were seeded in 35 mm confocal dishes and treated with various concentrations of **Ir3** for 24 h. The cells were then collected and stained with Annexin V and PI at room temperature in the dark for 15 min before being imaged by CLSM using a 100 × oil-immersion objective lens. The excitation/emission wavelength for Annexin V was set at 488/525 ± 25 nm.

Caspase-3/7 activity assay

A549 cells were seeded in white-walled nontransparent bottomed 96-well plates and treated with **Ir3** at different concentrations (0.5, 1.0, 2.0 μM). Following 24 h of incubation, the activity of caspase-3/7 was measured using the Caspase Glo® 3/7 Assay kit protocol, and luminescence was measured using a microplate reader (infinite M200 PRO, TECAN, Switzerland).

Western blotting analysis

The expression levels of A549 cells protein (cleaved caspase 3/9, PARP, cleaved-PARP) after the treatment with iridium complexes were detected by western blot following published methods.[70,74] The protein bands were visualized using ChemiDoc™ XRS þ Imaging System (Bio-Rad, USA).

3D multicellular tumor spheroids (MCTSs) formation

A sterilized PBS solution containing 0.75% agarose was added to each well of a 96-well plate at a volume of 50 mL per well. The plate was then cooled for 4 h under UV light irradiation. A cell suspension of A549 (3×10^3 cells per well) was seeded on top of the agarose and incubated for 1–2 days until MCTSs were formed. The generated MCTSs were cultured and stored in a cell incubator at 37 °C and 5% CO_2, with the medium replaced every 2 days. Image J software was used to calculate the diameter of each tumor spheroid.

Calcein AM/PI staining assay

Ir1-3 to MCTSs was evaluated using Calcein AM/PI double staining. MCTSs were prepared as described previously and treated with iridium complexes for 48 h. The treated MCTSs were then stained with Calcein AM (λ_{ex} = 488 nm, λ_{em} = 525 ± 25 nm), and PI (λ_{ex} = 535 nm, λ_{em} = 617 ± 36 nm). Imaging was performed using CLSM.

Supplementary material

Supplementary data are available at *Metallomics* online.

Acknowledgments

This research was funded by the National Natural Science Foundation of China (No. 21701034, 82101505), the Discipline Construction Project of Guangdong Medical University (No. 4SG23004G), the Science and Technology Program of Guangdong Province (No. 2019B090905011), the Science and Technology Program of Zhanjiang (No. 2021A05044, 2021A05242), the Medical Scientific Research Foundation of Guangdong Province of China (No. A2022026), the Zhanjiang Marine Young Talent Innovation Project (No. 2022E05013) and the University Student Innovation Experiment Program (No. S202210571061, ZZZF006). We thank the Public Service Platform of South China Sea for R&D Marine Biomedicine Resources for support.

Data availability

All data are incorporated into the article and its online supplementary material.

Conflicts of interest

There are no conflicts to declare.

References

1. F. Bray, M. Laversanne, E. Weiderpass and I. Soerjomataram, The ever-increasing importance of cancer as a leading cause of premature death worldwide, *Cancer*, 2021, 127 (16), 3029–3030.
2. B. V. Patel and J. M. Hotaling, Impact of chemotherapy on subsequent generations, *Urol. Oncol.*, 2020, 38 (1), 10–13.
3. N. Roy, U. Sen, Y. Madaan, V. Muthukumar, S. Varddhan, S. K. Sahoo, D. Panda, B. Bose and P. Paira, Mitochondria-targeting click-derived pyridinyltriazolylmethylquinoxaline-based Y-shaped binuclear luminescent ruthenium(II) and iridium(III) complexes as cancer theranostic agents, *Inorg. Chem.*, 2020, 59 (23), 17689–17711.
4. L. Qin, W. Yi, X. Y. Lian and Z. Z. Zhang, Bioactive alkaloids from the actinomycete actinoalloteichus sp. ZZ1866, *J. Nat. Prod.*, 2020, 83 (9), 2686–2695.
5. L. Tabrizi and F. Abyar, De Novo design of Cu(II) complex containing CNC-pincer-vitamin B3 and B7 conjugates for breast cancer application, *Mol. Pharm.*, 2019, 16 (9), 3802–3813.
6. Z. Y. Pan, C. P. Tan, L. S. Rao, H. Zhang, Y. Zheng, L. Hao, L. N. Ji and Z. W. Mao, Recoding the cancer epigenome by intervening in metabolism and iron homeostasis with mitochondria-targeted rhenium(I) complexes, *Angew. Chem. Int. Ed.*, 2020, 59 (42), 18755–18762.
7. R. R. Ye, W. Peng, B. C. Chen, N. Jiang, X. Q. Chen, Z. W. Mao and R. T. Li, Mitochondria-targeted artesunate conjugated cyclometalated iridium(iii) complexes as potent anti-HepG2 hepatocellular carcinoma agents, *Metallomics*, 2020, 12 (7), 1131–1141.
8. D. D. Paul Elisa and V. Vaidyanathan Ganesan, Switch-on effect on conformation-specific arylamine-DNA adduct by cyclometalated Ir(III) complexes, *J. Biol. Inorg. Chem.*, 2020, 25 (2), 305–310.
9. Z. Liu, A. Habtemariam, A. M. Pizarro, S. A. Fletcher, A. Kisova, O. Vrana, L. Salassa, P. C. Bruijnincx, G. J. Clarkson, V. Brabec and P. J. Sadler, Organometallic half-sandwich iridium anticancer complexes, *J. Med. Chem.*, 2011, 54 (8), 3011–3026.
10. H. W. Zhang, L. Tian, R. X. Xiao, Y. Zhou, Y. Y. Zhang, J. Hao, Y. J. Liu and J. P. Wang, Anticancer effect evaluation *in vitro* and *in vivo* of iridium(III) polypyridyl complexes targeting DNA and mitochondria, *Bioorg. Chem.*, 2021, 115, 105290.
11. L. M. Chen, J. Wang, X. H. Cai, S. X. Chen, J. J. Zhang, B. J. Li, W. G. Chen, X. H. Guo, H. Luo and J. C. Chen, Cyclometalated Ru(II)-isoquinoline complexes overcome cisplatin resistance of A549/DDP cells by downregulation of Nrf2 via Akt/GSK-3beta/Fyn pathway, *Bioorg. Chem.*, 2022, 119, 105516.
12. T. S. Kang, Z. F. Mao, C. T. Ng, M. Wang, W. H. Wang, C. M. Wang, S. M. Lee, Y. T. Wang, C. H. Leung and D. L. Ma, Identification of an iridium(III)-based inhibitor of tumor necrosis factor-alpha, *J. Med. Chem.*, 2016, 59 (8), 4026–4031.
13. H. J. Zhong, L. H. Lu, K. H. Leung, C. C. L. Wong, C. Peng, S. C. Yan, D. L. Ma, Z. W. Cai, H. M. David Wang and C. H. Leung, An iridium(iii)-based irreversible protein–protein interaction inhibitor of BRD4 as a potent anticancer agent, *Chem. Sci.*, 2015, 6 (10), 5400–5408.
14. W. W. Qin, Z. Y. Pan, D. H. Cai, Y. Li and L. He, Cyclometalated iridium(iii) complexes for mitochondria-targeted combined chemo-photodynamic therapy, *Dalton Trans.*, 2020, 49 (11), 3562–3569.
15. Y. Q. Wu, J. Wu and W. Y. Wong, A new near-infrared phosphorescent iridium(III) complex conjugated to a xanthene dye for mitochondria-targeted photodynamic therapy, *Biomater. Sci.*, 2021, 9 (14), 4843–4853.
16. S. Shamjith, M. M. Joseph, V. P. Murali, G. S. Remya, J. B. Nair, C. H. Suresh and K. K. Maiti, NADH-depletion triggered energy shutting with cyclometalated iridium (III) complex enabled bimodal luminescence-SERS sensing and photodynamic therapy, *Biosens. Bioelectron.*, 2022, 204, 114087.
17. X. C. Liu, Y. L. Han, X. X. Ge and Z. Liu, Imidazole and benzimidazole modified half-sandwich iridium(III) N-heterocyclic carbene complexes: synthesis, anticancer application, and organelle targeting, *Front. Chem.*, 2020, 8, 182.
18. J. Hao, H. W. Zhang, L. Tian, L. L. Yang, Y. Zhou, Y. Y. Zhang, Y. J. Liu and D. G. Xing, Evaluation of anticancer effects *in vitro* of new iridium(III) complexes targeting the mitochondria, *J. Inorg. Biochem.*, 2021, 221, 111465.
19. S. A. M. Khalifa, N. Elias, M. A. Farag, L. Chen, A. Saeed, M. F. Hegazy, M. S. Moustafa, A. Abd El-Wahed, S. M. Al-Mousawi, S. G. Musharraf, F. R. Chang, A. Iwasaki, K. Suenaga, M. Alajlani, U. Goransson and H. R. El-Seedi, Marine Natural Products: a source of novel anticancer drugs, *Mar. Drugs*, 2019, 17 (9), 491.
20. A. Mondal, S. Bose, S. Banerjee, J. K. Patra, J. Malik, S. K. Mandal, K. L. Kilpatrick, G. Das, R. G. Kerry, C. Fimognari and A. Bishayee, Marine cyanobacteria and microalgae metabolites-A rich source of potential anticancer drugs, *Mar.Drugs*, 2020, 18 (9), 476.
21. G. D. Demetri, M. von Mehren, R. L. Jones, M. L. Hensley, S. M. Schuetze, A. Staddon, M. Milhem, A. Elias, K. Ganjoo, H. Tawbi, B. A. Van Tine, A. Spira, A. Dean, N. Z. Khokhar, Y. C. Park, R. E. Knoblauch, T. V. Parekh, R. G. Maki and S. R. Patel, Efficacy and safety of Trabectedin or Dacarbazine for metastatic liposarcoma or leiomyosarcoma after failure of conventional chemotherapy: results of a phase III randomized multicenter clinical trial, *J. Clin. Oncol.*, 2016, 34 (8), 786–793.
22. P. A. Wender, C. T. Hardman, S. Ho, M. S. Jeffreys, J. K. Maclaren, R. V. Quiroz, S. M. Ryckbosch, A. J. Shimizu, J. L. Sloane and M. C. Stevens, Scalable synthesis of bryostatin 1 and analogs, adjuvant leads against latent HIV, *Science*, 2017, 358 (6360), 218–223.
23. Y. O. Ayipo, M. N. Mordi, M. Mustapha and T. Damodaran, Neuropharmacological potentials of beta-carboline alkaloids for neuropsychiatric disorders, *Eur. J. Pharmacol.*, 2021, 893, 173837.
24. Z. N. Wu, N. H. Chen, Q. Tang, S. Chen, Z. C. Zhan, Y. B. Zhang, G. C. Wang, Y. L. Li and W. C. Ye, Beta-carboline alkaloids from the seeds of Peganum harmala and their Anti-HSV-2 virus activities, *Org. Lett.*, 2020, 22 (18), 7310–7314.
25. I. Ahmad, S. Fakhri, H. Khan, P. Jeandet, M. Aschner and Z. L. Yu, Targeting cell cycle by beta-carboline alkaloids *in vitro*: novel therapeutic prospects for the treatment of cancer, *Chem. Biol. Interact.*, 2020, 330, 109229.
26. D. B. Zorov, M. Juhaszova and S. J. Sollott, Mitochondrial reactive oxygen species (ROS) and ROS-induced ROS release, *Physiol. Rev.*, 2014, 94 (3), 909–950.
27. D. C. Chan, Mitochondrial dynamics and its involvement in disease, *Annu. Rev. Pathol. Mech. Dis.*, 2020, 15 (1), 235–259.
28. F. J. Bock and S. W. G. Tait, Mitochondria as multifaceted regulators of cell death, *Nat. Rev. Mol. Cell Biol.*, 2020, 21 (2), 85–100.
29. C. Liu, X. C. Liu, X. X. Ge, Q. H. Wang, L. Zhang, W. J. Shang, Y. Zhang, X. A. Yuan, L. J. Tian, Z. Liu and J. M. You, Fluorescent iridium(iii) coumarin-salicylaldehyde schiff base compounds as lysosome-targeted antitumor agents, *Dalton Trans.*, 2020, 49 (18), 5988–5998.
30. H. Lu, X. P. Jiang, Y. Y. Chen, K. Peng, Y. M. Huang, H. Zhao, Q. Chen, F. T. Lv, L. B. Liu, S. Wang and Y. G. Ma, Cyclometalated iridium(iii) complex nanoparticles for mitochondria-targeted photodynamic therapy, *Nanoscale*, 2020, 12 (26), 14061–14067.

31. W. X. Zong, J. D. Rabinowitz and E. White, Mitochondria and cancer, *Mol. Cell*, 2016, 61 (5), 667–676.
32. W. G. Chen, X. H. Cai, Q. Sun, X. H. Guo, C. M. Liang, H. Tang, H. M. Huang, H. Luo, L. M. Chen and J. C. Chen, Design and synthesis of aptamer-cyclometalated iridium(III) complex conjugate targeting cancer cells, *Eur. J. Med. Chem.*, 2022, 236, 114335. https://doi.org/10.1016/j.ejmech.2022.114335.
33. J. C. Chen, F. Peng, Y. Zhang, B. J. Li, J. She, X. M. Jie, Z. L. Zou, M. Chen and L. M. Chen, Synthesis, characterization, cellular uptake and apoptosis-inducing properties of two highly cytotoxic cyclometalated ruthenium(II) beta-carboline complexes, *Eur. J. Med. Chem.*, 2017, 140, 104–117.
34. J. C. Chen, Y. Y. Deng, J. Wang, S. X. Chen, F. Peng, X. R. He, M. J. Liu, H. Luo, J. J. Zhang and L. M. Chen, Cyclometalated Ru(II) beta-carboline complexes induce cell cycle arrest and apoptosis in human HeLa cervical cancer cells via suppressing ERK and Akt signaling, *J. Biol. Inorg. Chem.*, 2021, 26 (7), 793–808.
35. R. Cao, J. l Jia, X. C. Ma, M. Zhou and H. Fei, Membrane localized iridium(III) complex induces endoplasmic reticulum stress and mitochondria-mediated apoptosis in human cancer cells, *J. Med. Chem.*, 2013, 56 (9), 3636–3644.
36. K. Lakshmi Manasa, S. Thatikonda, D. K. Sigalapalli, A. Sagar, G. Kiranmai, A. M. Kalle, M. Alvala, C. Godugu, N. Nagesh and B. Nagendra Babu, Design and synthesis of beta-carboline linked aryl sulfonyl piperazine derivatives: DNA topoisomerase II inhibition with DNA binding and apoptosis inducing ability, *Bioorg. Chem.*, 2020, 101, 103983.
37. W. Gu, I. Nusinzon, R. D. Smith, Jr., C. M. Horvath and R. B. Silverman, Carbonyl- and sulfur-containing analogs of suberoylanilide hydroxamic acid: potent inhibition of histone deacetylases, *Bioorg. Med. Chem.*, 2006, 14 (10), 3320–3329.
38. T. Suzuki, T. Kubota and J. Kobayashi, Eudistomidins H-K, new beta-carboline alkaloids from the Okinawan marine tunicate Eudistoma glaucus, *Bioorg. Med. Chem. Lett.*, 2011, 21 (14), 4220–4223.
39. R. C. Young, R. C. Mitchell, T. H. Brown, C. R. Ganellin, R. Griffiths, M. Jones, K. K. Rana, D. Saunders, I. R. Smith and N. E. Sore et al., Development of a new physicochemical model for brain penetration and its application to the design of centrally acting H2 receptor histamine antagonists, *J. Med. Chem.*, 1988, 31 (3), 656–671.
40. J. C. Thenmozhiyal, P. T. Wong and W. K. Chui, Anticonvulsant activity of phenylmethylenehydantoins: a structure-activity relationship study, *J. Med. Chem.*, 2004, 47 (6), 1527–1535.
41. C. A. Puckett and J. K. Barton, Fluorescein redirects a ruthenium-octaarginine conjugate to the nucleus, *J. Am. Chem. Soc.*, 2009, 131 (25), 8738–8739.
42. C. A. Puckett and J. K. Barton, Mechanism of cellular uptake of a ruthenium polypyridyl complex, *Biochemistry*, 2008, 47 (45), 11711–11716.
43. C. A. Puckett, R. J. Ernst and J. K. Barton, Exploring the cellular accumulation of metal complexes, *Dalton Trans.*, 2010, 39 (5), 1159–1170.
44. V. Pierroz, T. Joshi, A. Leonidova, C. Mari, J. Schur, I. Ott, L. Spiccia, S. Ferrari and G. Gasser, Molecular and cellular characterization of the biological effects of ruthenium(II) complexes incorporating 2-pyridyl-2-pyrimidine-4-carboxylic acid, *J. Am. Chem. Soc.*, 2012, 134 (50), 20376–20387.
45. S. Nikolic, L. Rangasamy, N. Gligorijevic, S. Arandelovic, S. Radulovic, G. Gasser and S. Grguric-Sipka, Synthesis, characterization and biological evaluation of novel Ru(II)-arene complexes containing intercalating ligands, *J. Inorg. Biochem.*, 2016, 160, 156–165.
46. J. J. Chen, Z. D. Luo, Z. N. Zhao, L. N. Xie, W. J. Zheng and T. F. Chen, Cellular localization of iron(II) polypyridyl complexes determines their anticancer action mechanisms, *Biomaterials*, 2015, 71, 168–177.
47. U. Schatzschneider, J. Niesel, I. Ott, R. Gust, H. Alborzinia and S. Wolfl, Cellular uptake, cytotoxicity, and metabolic profiling of human cancer cells treated with ruthenium(II) polypyridyl complexes [Ru(bpy)2(N—N)]Cl2 with N—N = bpy, phen, dpq, dppz, and dppn, *ChemMedChem*, 2008, 3 (7), 1104–1109.
48. J. C. Chen, Y. Zhang, X. M. Jie, J. She, G. Z. Dongye, Y. Zhong, Y. Y. Deng, J. Wang, B. Y. Guo and L. M. Chen, Ruthenium(II) salicylate complexes inducing ROS-mediated apoptosis by targeting thioredoxin reductase, *J. Inorg. Biochem.*, 2019, 193, 112–123.
49. L. M. Chen, F. Peng, G. D. Li, X. M. Jie, K. R. Cai, C. Cai, Y. Zhong, H. Zeng, W. Li, Z. Zhang and J. C. Chen, The studies on the cytotoxicity in vitro, cellular uptake, cell cycle arrest and apoptosis-inducing properties of ruthenium methylimidazole complex [Ru(MeIm)4(p-cpip)](2.), *J. Inorg. Biochem.*, 2016, 156, 64–74.
50. C. Y. Li, M. X. Yu, Y. S. Sun, Y. Q. Wu, C. H. Huang and F. Y. Li, A nonemissive iridium(III) complex that specifically lights-up the nuclei of living cells, *J. Am. Chem. Soc.*, 2011, 133 (29), 11231–11239.
51. C. Y. Li, Y. Liu, Y. Q. Wu, Y. Sun and F. Y. Li, The cellular uptake and localization of non-emissive iridium(III) complexes as cellular reaction-based luminescence probes, *Biomaterials*, 2013, 34 (4), 1223–1234.
52. C. L. Zhang, M. S. Liu, S. X. Liu, H. Yang, Q. Zhao, Z. P. Liu and W. J. He, Phosphorescence lifetime imaging of labile Zn(2+) in mitochondria via a phosphorescent iridium(III) complex, *Inorg. Chem.*, 2018, 57 (17), 10625–10632.
53. C. Ouyang, L. Chen, T. W. Rees, Y. Chen, J. K. Liu, L. N. Ji, J. G. Long and H. Chao, A mitochondria-targeting hetero-binuclear Ir(iii)-Pt(ii) complex induces necrosis in cisplatin-resistant tumor cells, *Chem. Commun.*, 2018, 54 (49), 6268–6271.
54. T. Meng, Q. P. Qin, Z. L. Chen, H. H. Zou, K. Wang and F. P. Liang, Cyclometalated Ir(III)-8-oxychinolin complexes acting as red-colored probes for specific mitochondrial imaging and anticancer drugs, *Eur. J. Med. Chem.*, 2020, 192, 112192.
55. N. Yoshinaga and K. Numata, Rational designs at the forefront of mitochondria-targeted gene delivery: recent progress and future perspectives, *ACS Biomater. Sci. Eng.*, 2022, 8 (2), 348–359.
56. X. L. Yi, Y. Yan, L. Li, R. Zhou, X. R. Shen and Y. Huang, Combination of mitochondria impairment and inflammation blockade to combat metastasis, *J. Control. Release*, 2022, 341, 753–768.
57. A. Perelman, C. Wachtel, M. Cohen, S. Haupt, H. Shapiro and A. Tzur, JC-1: alternative excitation wavelengths facilitate mitochondrial membrane potential cytometry, *Cell Death Dis.*, 2012, 3 (11), e430.
58. B. H. Xu, Z. P. Ding, Y. Hu, T. Zhang, S. L. Shi, G. M. Yu and X. C. Qi, Preparation and evaluation of the cytoprotective activity of micelles with DSPE-PEG-C60 as a carrier against doxorubicin-induced cytotoxicity, *Front. Pharmacol.*, 2022, 13, 952800.
59. J. C. Chen, Y. Zhang, B. J. Li, G. D. Li, X. M. Jie, Y. Cui, Z. L. Zou, X. F. Huang, J. Y. Qu and L. M. Chen, A comparative study on in vitro cytotoxicity, cellular uptake, localization and apoptosis-inducing mechanism of two ruthenium(II) complexes, *Transit. Met. Chem.*, 2018, 43 (2), 149–159.
60. N. Tanaka, Y. Honda, Y. Kajiwara, H. Kataoka, T. Origuchi, J. Sakamoto and M. Okita, Myonuclear apoptosis via cleaved caspase-3 upregulation is related to macrophage accumulation underlying immobilization-induced muscle fibrosis, *Muscle Nerve*, 2022, 65 (3), 341–349.

61. L. Y. Zhao, H. Y. Li, X. Huang, T. Liu, Y. Xin, Z. Q. Xiao, W. F. Zhao, S. Y. Miao, J. Chen, Z. B. Li and Y. Mi, The endocytic pathway of Pt nanoclusters and their induced apoptosis of A549 and A549/cis cells through c-myc/p53 and bcl-2/caspase-3 signaling pathways, *Biomed. Pharmacother.*, 2021, 144, 112360.
62. J. P. Liu, Y. Chen, G. Y. Li, P. Y. Zhang, C. Z. Jin, L. L. Zeng, L. N. Ji and H. Chao, Ruthenium(II) polypyridyl complexes as mitochondria-targeted two-photon photodynamic anticancer agents, *Biomaterials*, 2015, 56, 140–153.
63. F. Yang, J. R. Huang, H. X. Liu, W. Q. Lin, X. L. Li, X. Q. Zhu and T. F. Chen, Lentinan-functionalized selenium nanosystems with high permeability infiltrate solid tumors by enhancing transcellular transport, *Nanoscale*, 2020, 12 (27), 14494–14503.
64. S. Han, S. Kim, Z. Chen, H. K. Shin, S. Y. Lee, H. E. Moon, S. H. Paek and S. Park, 3D Bioprinted vascularized tumour for drug testing, *IJMS*, 2020, 21 (8), 2993.
65. A. Calcaterra, L. Mangiardi, G. Delle Monache, D. Quaglio, S. Balducci, S. Berardozzi, A. Iazzetti, R. Franzini, B. Botta and F. Ghirga, The pictet-spengler reaction updates its habits, *Molecules*, 2020, 25 (2), 414.
66. Z. B. Li, S. H. Chen, S. W. Zhu, J. J. Luo, Y. M. Zhang and Q. F. Weng, Synthesis and fungicidal activity of beta-carboline alkaloids and their derivatives, *Molecules*, 2015, 20 (8), 13941–13957.
67. A. Mattiuzzi, L. Marcelis, I. Jabin, C. Moucheron and A. Kirsch-De Mesmaeker, Synthesis and electrochemical and photophysical properties of calixarene-based ruthenium(II) complexes as potential multivalent photoreagents, *Inorg. Chem.*, 2013, 52 (19), 11228–11236.
68. L. He, K. N. Wang, Y. Zheng, J. J. Cao, M. F. Zhang, C. P. Tan, L. N. Ji and Z. W. Mao, Cyclometalated iridium(iii) complexes induce mitochondria-derived paraptotic cell death and inhibit tumor growth in vivo, *Dalton Trans.*, 2018, 47 (20), 6942–6953.
69. B. B. Chen, N. L. Pan, J. X. Liao, M. Y. Huang, D. C. Jiang, J. J. Wang, H. J. Qiu, J. X. Chen, L. Li and J. Sun, Cyclometalated iridium(III) complexes as mitochondria-targeted anticancer and antibacterial agents to induce both autophagy and apoptosis, *J. Inorg. Biochem.*, 2021, 219, 111450.
70. J. C. Chen, J. Wang, Y. Y. Deng, T. Wang, T. F. Miao, C. P. Li, X. H. Cai, Y. Liu, J. Henri and L. M. Chen, Ru(II) complexes bearing O, O-chelated ligands induced apoptosis in A549 cells through the mitochondrial apoptotic pathway, *Bioinorg. Chem. Appl.*, 2020, 2020, 1.
71. R. L. Guan, Y. Chen, L. L. Zeng, T. W. Rees, C. Z. Jin, J. J. Huang, Z. S. Chen, L. N. Ji and H. Chao, Oncosis-inducing cyclometalated iridium(iii) complexes, *Chem. Sci.*, 2018, 9 (23), 5183–5190.
72. B. Yuan, J. P. Liu, R. L. Guan, C. Z. Jin, L. N. Ji and H. Chao, Endoplasmic reticulum targeted cyclometalated iridium(iii) complexes as efficient photodynamic therapy photosensitizers, *Dalton Trans.*, 2019, 48 (19), 6408–6415.
73. J. J. Cao, C. P. Tan, M. H. Chen, N. Wu, D. Y. Yao, X. G. Liu, L. N. Ji and Z. W. Mao, Targeting cancer cell metabolism with mitochondria-immobilized phosphorescent cyclometalated iridium(iii) complexes, *Chem. Sci.*, 2017, 8 (1), 631–640.
74. J. C. Chen, Y. Zhang, G. D. Li, F. Peng, X. M. Jie, J. She, G. Z. Dongye, Z. L. Zou, S. W. Rong and L. M. Chen, Cytotoxicity *in vitro*, cellular uptake, localization and apoptotic mechanism studies induced by ruthenium(II) complex, *J. Biol. Inorg. Chem.*, 2018, 23 (2), 261–275.

Received: March 29, 2023. **Accepted:** May 17, 2023